NANO-MICROCOMPOSITE AND COMBINED COATINGS ON Ti-Si-N/WC-Co-Cr/STEEL AND Ti-Si-N/$(Cr_3C_2)_{75}$-$(NiCr)_{25}$ BASE: THEIR STRUCTURE AND PROPERTIES

N.K. Erdybaeva

East-Kazahstan State University of Technology, Ust'-Kamenogorsk Kazahstan

Received 21.06.2010

Two types of nano-microcomposite coatings Ti-Si-N/WC-Co-Cr and Ti-Si-N/$(Cr_3C_2)_{75}(NiCr)_{25}$ of 160 to 320 jm thickness were manufactured using two deposition technologies: cumulative-detonation and vacuum-arc deposition in HF discharge. The combined coatings restored worn areas of tools and demonstrated high corrosion and wear resistance, increased hardness, elastic modulus, and plasticity index. The composition of top coating changed from Ti = 60 at.%, N ≈ 30 at.%, and Si ≈ 5 at.% to N = 20 at.% and Ti – the rest. The first series of coatings indicated the following phases: (Ti, Si)N and TiN for thin coating and WC, W_2C for thick one.

The second series indicated (Cr_3Ni_2), pure Cr, and little amount of $Ti_{19}O_{17}$ (in transition region) for thick coating and (Ti, Si)N, TiN for thin one.

For the first series, grain sizes reached 25nm, hardness was 38 GPa., elastic modulus E = (370 + 32) GPa, and plasticity index H/E = 0,11 – 0,12 For the second series, grain sizes were 15 nm, hardness essentially exceeded 42 GPa ± 4 GPa, elastic modulus E = (425 + 38) GPa, and plasticity index H/E = 0,12 – 0,13. Corrosion resistance in salt solution and acidic media increased and cylinder-surface friction wear decreased.

Keywords: nanocomposite,cumulative-detonation, vacuum-arc deposition, corrosion resistance, elastic modulus

Отримано два види комбінованих нанокомпозитних покриттів (Ti-N-Si/WC-Co-Cr; TI-N-Si/$(Cr_3C_2Ni)_{75}$-$(NiCr)_{25}$) товщиною 160 ё 320 мкм з використанням двох технологій осадження: кумулятивно-детонаційним з подальшим осадженням за допомогою вакуумно-дугового джерела у ВЧ розряді. Що дає можливість, за допомогою комбінованого покриття, відновлювати розмір зношених ділянок виробів із захистом їх від корозії, зносу, при цьому збільшити твердість, модуль пружності, індекс пластичності. Склад верхнього покриття змінювали від Ti = 60%, N ≈30%, Si = 10% до Si = 5%; N = 20%, Ti = 75%. У першій серії покриттів виявлені фази (Ti, Si) і TiN в тонкому верхньому покритті і WC і W_2C в товстому нижньому покритті.

У другій серії, у верхньому покритті були отримані (Ti, Si) N і TiN, а в нижньому покритті Cr_3Ni_2, чистий Cr; невелика кількість $Ti_{19}O_{17}$ в перехідній області між тонким і товстим покриттям.

Розмір зерен в першому варіанті тонкого покриття складав 25 нм, при твердості 35 ГПа, а в другому варіанті розмір зерен кристалітів складав 15 нм при твердості H = 42 ± 3,6 ГПа. Показано, що корозійна стійкість в сольовому розчині і кислотному середовищах збільшується, при зменшенні зносу в результаті тертя циліндра по поверхні комбінованого покриття.

Ключові слова: нанокомпозитні покриття, кумулятивна детонація, вакуумно-дугове осадження, модуль пружності, індекс пластичності, корозійна стійкість.

Получено два вида комбинированных нанокомпозитных покрытий (Ti-N-Si/WC-Co-Cr; Ti-N-Si/$(Cr_3C_2Ni)_{75}$-$(NiCr)_{25}$) толщиной 160 ÷ 320 мкм с использованием двух технологий осаждения: кумулятивно-детонационным с последующим осаждением с помощью вакуумно-дугового источника в ВЧ разряде. Что даёт возможность, при помощи, комбинированного покрытия восстанавливать размер изношенных участков изделий с защитой их от коррозии, износа, при этом увеличить твердость, модуль упругости, индекс пластичности. Состав верхнего покрытия изменяли от Ti = 60%, N ≈ 30%, Si = 10% до Si = 5%; N = 20%, Ti = 75%. В первой серии покрытий обнаружены фазы (Ti; Si) и TiN в тонком верхнем покрытии и WC и W_2C в толстом нижнем покрытии.

Во второй серии, в верхнем покрытии были получены (Ti, Si)N и TiN, а в нижнем покрытии Cr_3Ni_2, чистый Cr; небольшое количество $Ti_{19}O_{17}$ в переходной области между тонким и толстым покрытием.

Размер, зерен в первом варианте тонкого покрытия, составлял 25 нм, при твёрдости 35 ГПа, а во втором варианте размер зёрен кристаллитов составлял 15 нм при твёрдости H = 42 ± 3,6 ГПа. Показано, что коррозионная стойкость в солевом растворе и кислотной средах увеличивается при уменьшении износа в результате трения цилиндра по поверхности комбинированного покрытия.

Ключевые слова: нанокомпозитные покрытия кумулятивная детонация, вакуумно-дуговое осаждение, модуль упругости, индекс пластичности, коррозионная стойкость.

INTRODUCTION

Nanocomposite materials as a class of nanomaterials is characterized by a heterogeneous structure, which was formed by practically non-interacting phases with grain dimensions 5 to 35 nm [1 – 3]. As a rule, components of such structures are amorphous matrix and inclusions of nanocrystalline phases. These amorphous components agree in the best way with nanocrystalline surfaces providing good adhesion and essentially increasing hardness. Small grain dimensions of the second phase in combination with good strength of intergrain boundaries provide high mechanical properties of such composition materials.

Today, nanomaterials are divided into three classes according to their hardness values: hard nanocomposites of ≥ 20 to 40 GPa hardness, superhard of 40 to 80 GPa, and ultrahard of ≥ 80 GPa [3 – 4]. In addition to protecting functions, chemical and machine building industries need restoration of initial tool dimensions for those tools, which already are functioning in industry. For these purposes, tools are coated with thick coatings, the physical and mechanical properties of which are higher than those of a basic material. Usually, alloys (powders) Ni-Cr-Mo [5], hard alloys WC-Co-Cr [6, 8] and Cr_3C_2-Ni, and oxide ceramics Al_2O_3, Al_2O_3-Cr_2O_3 [5, 7] are used for such coatings.

In such a way, a combination two layers, for example a thick layer of WC-Co-Cr hard alloy of 100 μm, which was formed using cumulative or detonation deposition, and Ti-Si-N thin upper layer (units of a micron) with enhanced physical-mechanical characteristics, which was formed by subsequent condensation, was able to provide higher protecting functions and restore worn surface regions.

The aim of this work was manufacturing of Ti-Si-N-, Ti-Si-N/WC-Co-Cr- and Ti-Si-N/$(Cr_3C_2)_{75}$-$(Ni\text{-}Cr)_{25}$– based coatings and investigation of their physical and mechanical properties.

EXPERIMENTAL DETAILS

Polished samples of St. 45 (0.45%C, Fe the rest) of 4 mm and 20 mm diameter were coated using vacuum-arc source with high-frequency discharge. Ti alloyed sintered cathode containing 5 to 10 wt.% of Si was deposited using the Bulat 3T-device functioning under $5 \cdot 10^{-5}$ Pa vacuum and 100 A cathode current. The sputtering was carried out using two regimes: the standard vacuum-arc method, and HF-regime. A bias potential was applied to the substrate from a HF generator, which produced impulses of convergent oscillations with ≤ 1 MHz frequency, every impulse duration being 60 μs, their repetition frequency – about 10 kHz. Due to HF diode effect the value of negative auto bias potential occurring in the substrate amounted to 2 to 3 kV at the beginning of impulse (after start of a discharger operation). Coatings of 2 to 3.5 μm thickness were deposited to steel substrates of 20 and 30 mm diameter, and 3 to 5 mm thickness without additional substrate heating. A molecular nitrogen was employed as a reactive gas The first series of rounded steel 3 (0.3 wt.%C) samples of 20 mm diameter and 4 to 5mm thickness was deposited using cumulative-detonation device CDS-1 of the following parameters: 65 mm distance to a nozzle cut, 14 mm/s displacement velocity, 5 runs, 12Hz pulse repetition frequency (for WC-Co-Cr). After the deposition, the 160 to 320jm thick coating was melted by a plasma jet (without powder) using eroding W electrode. A melted layer thickness was 45 to 60 μm. Then, Ti-Si-N thin coating of about 3 μm was deposited over the thick one using the same device Bulat 3T (the method was described above).

For the second series of samples, powder mixture $(Cr_3C_2)_{75}$-$(NiCr)_{25}$ was used, with powder size of 37.8 μm. The distance to a nozzle was 70 mm, displacement velocity – 4 mm/sec, 4 passed, pulse repetition frequency was 12Hz, capacity was C = 200 μF, and capacity battery was 3.2 kV.

For Bulat 3T, conditions for thin coating deposition remained the same.

For element analysis, we applied the following methods: Rutherford back-scattering of $^4He^+$ of 1.76MeV energy (RBS), scanning electron microscopy (SEM) with EDS (REMMA-103M, Selmi, Ukraine), X-ray diffraction (DRON-3 and Advantage 8, USA).

Hardness and elastic modulus were measured using nanoindentation device Nanoindenter II, MTS System Corporation, Oak Ridge TN (USA) with Berkovich pyramid. Elastic modulus was determined using "load-unload" curves, according to Oliver-Pharr method [14]. Scanning tun-

neling microscope (STM) of 1nm resolution was used to study the thin layer surface morphology.

RESULTS AND DISCUSSIONS

The cumulative-detonation device functioned under conditions of detonation burning of combustion gaseous mixtures. The device (fig. 1) was constructed of the following sites.

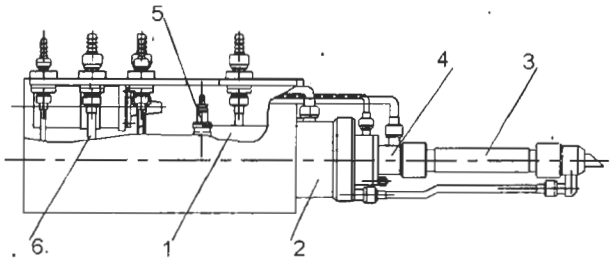

Fig. 1. The cumulative-detonation device.

A system of pipelines was used to feed components of combustion gaseous mixtures. Basic difference between cumulative-detonation and detonation devices is that the former realized summary energies of detonation combustion products from several specially designed chambers. Cumulative energy allows high-velocity gas flow with several shock waves providing efficient interaction with powder material. In this way, energy of combustion mixtures is rationally used. The rate and temperature of combustion products depend only on combustion conditions in every chamber. Nozzles function not less than 1000 hours. High burning frequency of 15 to 30 Hz is able to provide quasicontinuous coating deposition.

To increase potential of a technological system, generator allowing one to reach up to 100 kW impulse of high-frequency (HF) discharge was constructed on the basis of pulsed generator with impact contouring. It allowed one to obtain a single pulse of high power under low impedance load, in other words, to operate in a 'shot circuiting' mode.

An advantage of such generators is that their operation weakly depended on changes of loading impedance, which was principally important for functioning under pulsed mode under pulsed loading. To hold up HF discharge, one needed high voltage, which would increase absorption of HF power in discharge. Therefore, in operations with high voltage and high capacity (high current), a special discharge unit would serve as a special commutator.

Discharge started at aluminum coils, then it displaced to copper electrodes having good heat conductivity. The discharge unit had special holes for air cooling of plates. Application of such construction provided high voltages and current and generator operation stability. Spark resistance of discharge units was calculated using perfect Tamppler formula [13]

$$R = 2.510^{-8}\ f/c, \qquad (1)$$

where c – is capacity value, which was discharged with f discharge frequency.

Fig. 2a shows a scheme for tested generator with f_o = 300 kHz, ρ = –10 Ohm, $C = T_{pl}$, L = 5 μG, U_o = 10 kV, t_{ipl} = 30 js, stored capacitor energy was E_o = 2,5 J, pulsed power P_{pulse} = 8.3 kW. The calculation demonstrated that under periodical discharge t_{pulse} = 1.5 μs, P_{pulse} = 1.6 MW, repetition frequency f = 3.0 kHz, t_{rep} = 330 μs, an average power P = 7.5 kW, discharge current $I = 10^3$ A.

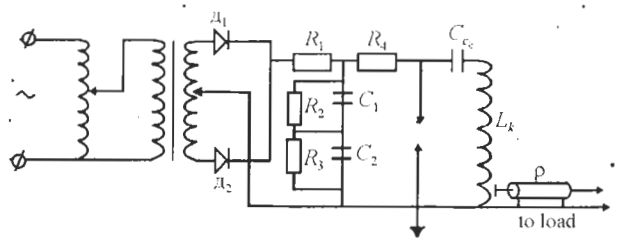

Fig. 2a. A scheme of an impact HF generator, which switched plasma-producing antennae, operated in two modes: 1) with an open input (ohmic circuit – zero distance between antenna and ground) and 2) with a closed input – the antenna was separated from the ground by a capacity.

Charged plasma particles in electric HF field of the antennae E reached the following velocity:

$$V = \frac{eE}{mw}, \qquad (2)$$

where e – is a particle charge, m – is particle mass, w – is cyclic generator frequency.
Then, particle range in a field E and under w frequency will be

$$Z_{\max} = \frac{eE}{mw^2}. \qquad (3)$$

Selecting E and f such that an electron range amounted several centimeter (cm), ion remaining practically non-mobile, the antenna HF voltage started to be detected by a plasma.

Under closed input mode, the antenna was negatively charged, and under open input mode, electrons left the zone of antenna.

Without external magnetic field this zone is:

$$\delta \approx \frac{C}{2\pi \cdot 10^4 \sqrt{n_e}}, \qquad (4)$$

where c – is light velocity; n – is plasma density.

Under action of positive potential ions gained energy for directed motion and bombarded the antenna (under closed input mode) or an internal surface of vacuum chamber and its inside content. This bombardment cleaned the antenna surface, chamber, and tools inside. Ion energy may be controlled by drawing a fraction of charges aside of the antennae by switching higher resistance.

In this case, material sputtering occurred. Maximum voltage amplitude at the beginning of HF impulse was determined by energy value of concrete ions under action of this electric field and by corresponding sputtering efficiency of coated material. The technological device [7, 14] was constructed on the basis of vacuum chamber (7). Grounded metallic walls of vacuum chamber served simultaneously like an anode of vacuum-arc discharge system. Negative potential from an arc-discharge feeding source was applied to a cathode (4), which was fabricated from a material desired for further coating synthesis. A working gas was fed through a gas line (5) using a leak system (1). For additional chemical activation, molecular gases were fed to the vacuum chamber. They passed through a cylindrical quartz discharge chamber (11), in which a generator (12) produced periodically repeated spark discharges. Tools were arranged on a movable table (8). HF voltage was applied to a substrate (8) through the matching device (9) from the HF generator.

In such a way, working with decreasing voltage (fig. 2b) during every impulse, one can join two main technological operations of coating deposition (clearing and deposition), which earlier were performed separately using devices for vacuum-arc deposition. This allowed one to choose better conditions for coating deposition and saved time. Depositing Al_2O_3 and TiN coatings, it was demonstrated that changing HF voltage potential applied to substrate, one could affect coating phase composition [14, 15].

Fig. 3 presents an image of nano-microcomposite surface for combined Ti-Si-N/WC-Co-Cr coating.

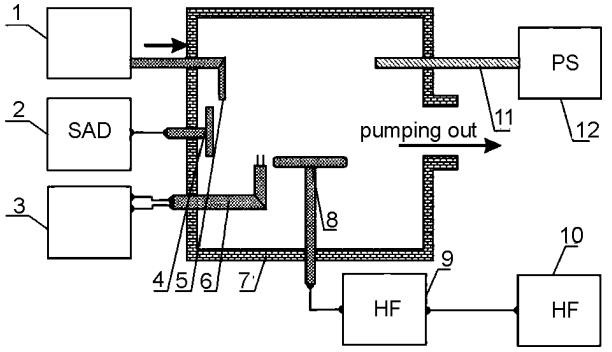

Fig. 2b. A scheme of a technological system for coating synthesis operating on the basis of a vacuum-arc discharge: 1 is a device for gas-feeding; 2 – sources for arc-discharge feeding; 3 – measuring probe; 4 – a cathode; 5 – a gas line for gas-feeding; 6 – a double movable probe; 7 – a vacuum chamber; 8 – a substrate; 9 – a device to match a HF-generator; 10 – the HF-generator; 11 – a quartz tube for dissociation of working gas molecules; 12 – power source.

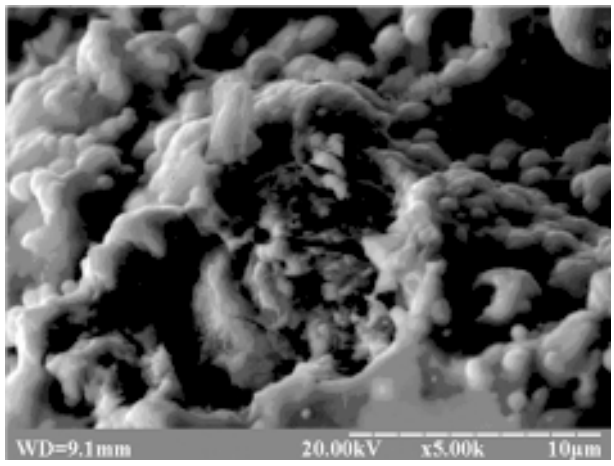

Fig. 3. Images of surface regions for nano-microcomposite combined coating Ti-Si-N/$(Cr_3C_2)_{75}$-$(NiCr)_{25}$.

Fig. 4a presents RBS data for the thick WC-Co-Cr coating without Ti-Si-N thin one.

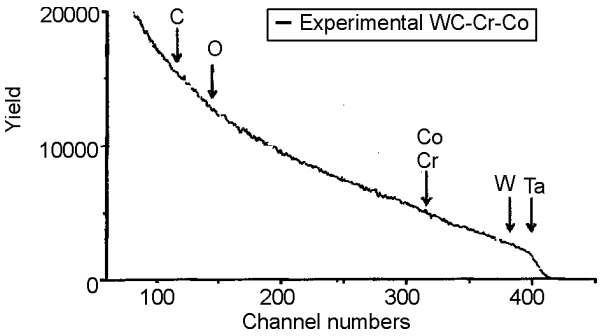

Fig. 4a. Energy spectra of Rutherford ion backscattering (RBS) for thick coating WC-Co-Cr.

A thin coating was formed using vacuum-arc source and followed the coating surface relief formed by plasma-detonation. Its average roughness varies from 14 to 22 μm (after melting and coating deposition using vacuum-arc source). An image of X-ray energy dispersion spectrum is presented below. It indicates the following ele-

ment concentrations in the thin coating: N ~ 7.0 to 7.52 vol.%; Si ~ 0.7vol.%; Ti ~ 76.70 to 81 vol.%. For the thick coating we found Fe ~ 0.7 vol.%, and traces of Ni and Cr.

Results for combined coating are presented below, fig.4b.

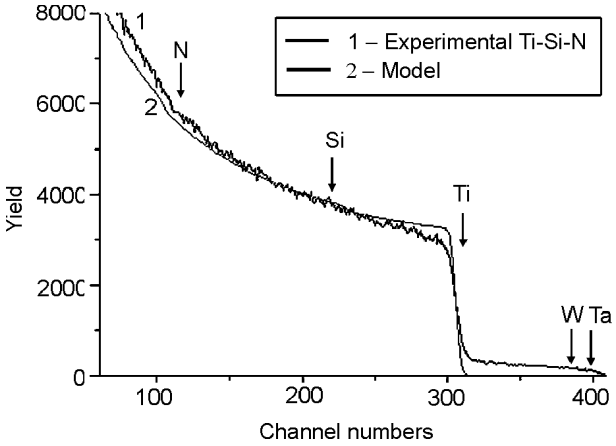

Fig. 4b. Energy spectra of Rutherford ion backscattering (RBS) for top thin coating Ti-Si-N/WC-Co-Cr.

Element distribution, which was calculated according to a standard program [5], indicated N = 30 at.%; Si ≈ 5 to 6 at.%; Ti ≈ 63 to 64 at.%. Spectrum of thick coating did not allow us to evaluate element concentration due to high surface roughness of the coating formed by plasma-detonation method.

X-ray analysis of a combined nanocomposite coating is shown in fig. 5.

It indicates the following phases: (Ti, Si)N; TiN – for thin coating, and WC; W_2C – for thick one.

Special samples were prepared for hardness measurements. Their surfaces were grinded and then polished. After grinding, thickness of WC-Co-Cr thick coating decreased to 80 – 90 μm. Thin Ti-Si-N film of about 3 μm was condensed

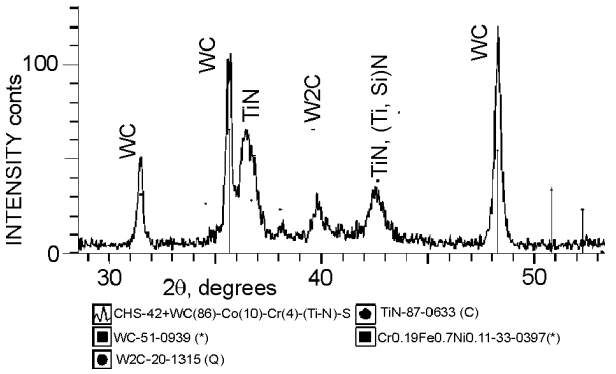

Fig. 5. Diffraction patterns fragments obtained for surface region of nano-microcomposite combined coating Ti-Si-N/WC-Co-Cr/steel substrate.

to the grinded surface. As a result, we found that hardness of different regions essentially varied within 29 ± 4GPa to 32 ± 6GPa. Probably, it is related to non-uniformity of plasma-detonation coating surface, which hardness varied up 11.5 to 17.3 GPa. These hardness values remained after condensation of Ti-Si-N thin coating Elastic modulus also features non-ordinary behavior.

Hardness of the thin coating, which was deposited to a polished steel St.45(0.45%C) surface had maximum value of 48GPa, and its average value H_{av} was 45 GPa. Variation of hardness values was lower than that found in a combined coating.

Fig. 6 shows dependences of loading-unloading for various indentation depths.

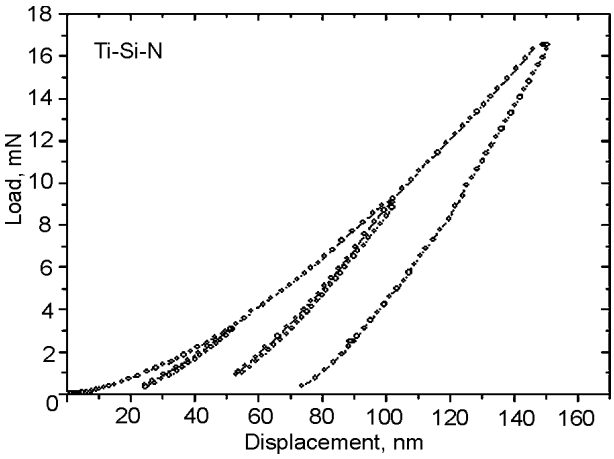

Fig. 6. Loading-unloading curves for Ti-Si-N/WC-Co-Cr coating under various Berkovich indentation depths.

These dependences and calculations, which were performed according to Oliver-Pharr technique [14], indicated that hardness of Ti-Si-N coatings deposited to thick $(Cr_3C_2)_{75}$-$(NiCr)_{25}$ was 37.0 ± 4.0 GPa under E = 483 GPa.

Fig. 7 shows fragments of diffraction patterns for nano-microcomposite combined coating Ti-Si-N/$(Cr_3C_2)_{75}$-(Ni-Cr)$_{25}$.

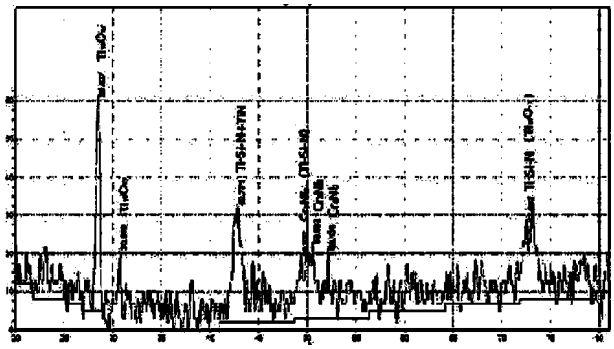

Fig. 7. Diffraction patterns for combined nano-microcomposite coating Ti-Si-N/$(Cr_3C_2)_{75}$-$(NiCr)_{25}$.

Table 1

Calculation results for coating parameters and structures

№	Angle	Area	Intensity	Half-width	Interplanar	% max	Phase	*hkl*
1	28,437	8,511	37	0,4512	3,6416	100,00	Ti_9O_{17}	106 004
2	30,648	3,083	13	0,4518	3,3845	36,84	Ti_9O_{17}	0210 123
3	42,771	10,885	20	1,0490	2,4530	65,79	Ti-Si-N+TiN	111 111
4	49,332	13,862	13	1,9890	2,1413	34,21	Cr_3Ni_2 Ti-Si-N	321 200
5	49,993	17,418	15	2,2322	2,1168	34,47	TiN Ti_9O_{17}	200 1223 110
6	50,533	6,528	12	1,0335	2,0956	44,74	Cr_3Ni_2	330
7	52,134	2,782	15	0,3553	2,0355	39,47	Cr_3Ni_2 Cr Ni	202 110 111
8	72,500	18,056	18	1,8950	1,5127	47,37	Ti_9O_{17} Ti-Si-N	3130 220
9	73,040	11,106	13	1,5950	1,5030	52,63	TiN	220

These diffraction patterns and calculations of coating structure parameters are presented in tabl. 1.

In the coating, basic phases are Cr_3Ni_2 for the bottom thick coating and (Ti, Si)N and TiN for the thin top coating. Diffraction patterns were taken under cobalt emission. Additionally, we found phases of pure Cr and low concentration of titanium oxide (Ti_9O_{17}) at interphase boundary between thin-thick coatings. Peaks of Ti-Si-N and TiN coincided because of low Si content. (Ti, Si)N is solid solution based on TiN (Si penetration). The phases are well distinguished at 72 to 73° angles.

Fig. 8 shows regions of thick bottom $(Cr_3C)_{75}$-$(NiCr)_{25}$ coating and intensity distribution of X-ray emission for basic elements.

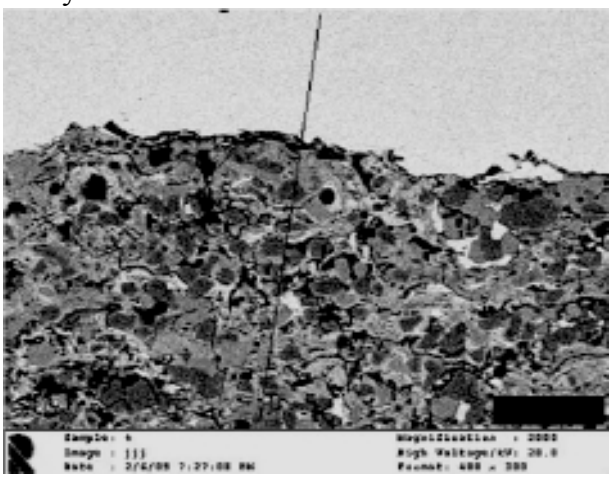

Fig. 8a. Regions of transversal cross-section for combined coatings (lines of element analysis are indicated) from SEM and EDS analyses.

In this coating, content of basic elements is the following: nickel and chromium – 36 wt.% and 64 wt.%, respectively. Also, we found carbon, oxygen, and silicon.[17, 18] Transversal cross-sections did not allow us to distinguish thin upper coating due to its low thickness. We found regions for pure nickel and chromium. Nickel matrix (a white region) indicated high amount of chromium inclusions with various grain dimensions: small grains of < 1 μ*m*, average – of 4 to 5 μ*m*, and big – of 15 to 20 μ*m*.

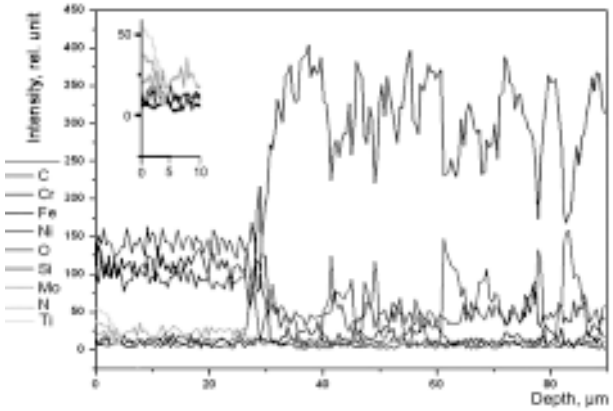

Fig. 8b. Element distribution over depth of combined coating Ti-Si-N/$(Cr_3C_2)_{75}$-$(NiCr)_{25}$ for the regions indicated in fig.8a.

The white region is reach in Ni (to 90at.%). A grey region is reach in Cr (to 92at.%). In these experiments. The inset of fig. 8 shows higher resolution element composition distribution in Ti-Si-N/$(Cr_3C_2)_{75}$-$(NiCr)_{25}$ nano-microcomposite

coating. In a thin nano-composite layer, one can see high Ti concentration, presence of Si, and high enough nitrogen content exceeding 6.7 wt.%.

Fig. 9 shows results of wear resistance tests, which were performed according to a scheme "cylinder-plane".

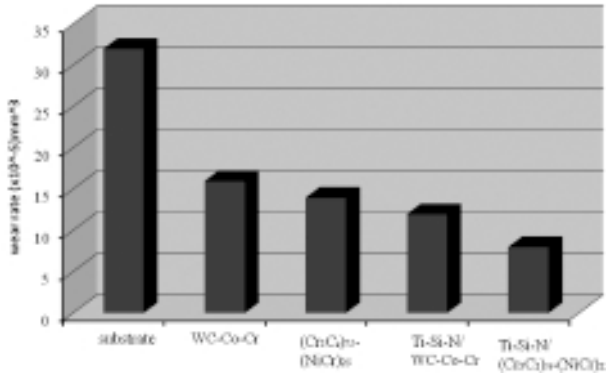

Fig. 9. Histograms of dependences of wear rates for samples, which were fubricated according to scheme cylinder-plane.

These results demonstrated the lowest friction wear for Ti-Si-N/$(Cr_3C_2)_{75}$-$(NiCr)_{25}$ system and the highest friction wear for substrate.

Adhesion between thin Ti-Si-N coating and thick $(Cr_3C_2)_{75}$-$(NiCr)_{25}$ one was 1.75 times higher than between Ti-Si-N and WC-Co-Cr. In addition, adhesion between thick $(Cr_3C_2)_{75}$-$(NiCr)_{25}$ coating and steel (substrate) was 7.2 times higher and more than 12.5 times higher than between thick WC-Co-Cr coating and steel (substrate). Maximum adhesion value of about 292N/m was found in the case of Ti-Si-N '! $(Cr_3C_2)_{75}$-$(NiCr)_{25}$.

CONCLUSION

Thick (> 100 jm) nanocomposite coatings of Ti-Si-N/WC-Co-Cr and Ti-Si-N/$(Cr_3C_2)_{75}(NiCr)_{25}$ compositions were formed and investigated.

In the first series of samples, thin coatings contained (Ti, Si)N and TiN phases. Grain dimensions were about 25 nm. Hardness reached 38 GPa.

In the second series of samples, in thin coating grain dimensions were smaller – about 15 nm. Hardness reached 42 to 44 GPa. Phase composition was the same – (Ti, Si)N and TiN. Si and N concentrations changed from 10 at.% to 5 at.% for Si and from 30 at.% to 20 at.% for N.

Wear resistance increased essentially, which was demonstrated by cylinder-to-sample surface friction. Corrosion resistance and other mechanical characteristics also increased.

ACKNOWLEDGEMENTS

The work was supported by projects ISTCs K-1198 and NAS of Ukraine "Nanosystems, Nanocoatings, Nanomaterils".

The author acknowledge Drs.S.B.Kislitsyn, Yu.Zh.Tuleushev from Institute for Nuclear Physics, NNC, Almaty,Prof A.D.Pogrebnjak from Sumy State University,Sumy Institute for Surface Modification, Prof. F.F. Komarov from Belarus State University, Minsk for their help in RBS analysis and corrosion tests.

REFERENCES

1. Pogrebnjak A.D., Shpak A.P., Azarenkov N.A., Beresnev V.M. Structures and Properties of Hard and Superhard Nanocomposite Coatings//Usp. Phys. – 2009. – Vol. 170, No. 1. – P. 35-64.
2. Musil J., Zeman P. Hard a-Si_3N_4/MeNx Nanocomposite Coatings With High Thermal Stability and High Oxidation Resistance//Solid State Phenome. – 2007. – Vol. 127. – P. 31-37.
3. Zhang R.F., Argon A.S., Veprek S. Electronic Structure, Stability, and Mechanism of the Decohesion and Shear of Interfaces in Superhard Nanocomposites and Heterostructures//Phys. Rev. – 2009. – Vol. B79. – P. 24542.
4. Veprek S., Veprek-Heijman M., Karvankova P., Prochazka J. Different approaches to superhard coatings and nanocomposites//Thin Solid Films. – 2005. – Vol. 476. – P. 1-25.
5. Musil J., Dohnal P., Zeman P. Physical Properties and High-Temperature Oxidation Resistance of Sputtered Si_3N_4/MoN_x Nanocomposite Coatings//J. Vac. Sci. Technology. – 2005. – Vol. 23, № 4. – P. 1568-1574.
6. Uglov V., Anishcik V., Zlotski S., Abadias G., Dub S.N. Structural and Mechanical Stability Upon Annealing of Arc-Deposited Ti-Zr-N Coatings//Surf. & Coat. Tech. 2008. – Vol. 202. – P. 2394-2398.
7. Azarenkov N.A., Beresnev V.M., Pogrebnjak A.D. Structure and Properties of Coatings and Modified Layers of Materials. – Kharkov: KhNU, 2007. – 565 p.
8. Nanostructure Coating/Eds. A.Gavaleiro, J.T. De Hosson.– Berlin: Springer-Verlag, 2006.– 340 p.

9. Musil J. Physical and Mechanical Properties of Hard Nanocomposite Films Prepared by Reactive Magnetron Sputtering. Ch. 10/Eds. A. Cavaleiro, J.Th.M. De Hosson. – Kluwer Academic/ Plenum Publishers. (N.-Y. USA), 2005.
10. Vishniakov Ja.D. Sovremennye Metody Issledovaniia Struktury Deformirovannykh Kristallov.– M.: Metallurgija, 1975. – 480 p.
11. Beresnev V.M., Pogrebnjak A.D., Kirik G.V., Edyrbaeva N.K., Ponaryadov V.V. Structure, and Properties and Fabrication of the Solid Nanocrystalline Coating in Several Ways//Progress in Physics of Metals. – 2007. – Vol. 8., No. 3. – P. 171-246.
12. Pogrebnjak A., Danilionok M., Uglov V., Erdybaeva N., Kirik G., Dub S., Rusakov V., Shypylenko A., Zukovski P., Tuleushev Y. Nanocomposite Protective Coatings Based on Ti-N-Cr/Ni-Cr-B-Si-Fe, Their Structure and properties//Vacuum. – 2009. – Vol. 83. – P. S235-S239.
13. Musil J. Physical and Mechanical Properties of Hard Nanocomposite Films Prepared by Reactive Magnetron Sputtering: invited Chapter 10. – Kluwer Academic/Plenum Pullishers, New York, 2007.
14. Kadyrzhanov K., Komarov F., Pogrebnjak A., et al. Ion-Beam Plasma Modification of Materials. – M.: MSU, 2005. – 640 p.
15. Beresnev V.M., Tolok V.T., Shvets O.M., Fursova E.V., Chernyshev, Malikov L.V. Micro-nanolayers coatings fabricated by vacuum-arc source with discharge//PSE.– 2006.–Vol. 4.– P. 104-109.
16. Pogrebnjak A.D., Shpak A.P., Beresnev V.M. New Nanotechniques Structure and Properties of Protective Composite Coatings and Modified Surface Prior and After Plasma High Energy Jets Treatment. Chapter 2/Eds. A. Malik, R.J. Rawat. – Nova Science Publ.New-York, 2009. – P. 21-115.
17. Pogrebnjak A.D. Metastable States and Structural Phase Changes in Metals andAlloys Exposed to High Power Pulsed Ion Beams//Phys. Stat. Sol. – 1990. – Vol. A117. – P. 17-49.
18. Pogrebnjak A.D., Remnev G.E. Plotnikov S.V. High-Power Ion-Beam-Induced and Mixing in Deposited Structures//Mater. Sci. and Engineer. – 1989. – Vol. A115. – P. 175-179.